Appl. Phys. B (2014) 117:75–84
DOI 10.1007/s00340-014-5801-6

Applied Physics B
Lasers and Optics

Optical and luminescence properties of Dy^{3+} ions in K–Sr–Al phosphate glasses for yellow laser applications

K. Linganna · P. Haritha · K. Venkata Krishnaiah · V. Venkatramu · C. K. Jayasankar

Received: 9 August 2013 / Accepted: 11 February 2014 / Published online: 6 May 2014

Abstract Trivalent dysprosium (Dy^{3+})-doped K–Sr–Al phosphate glasses have been prepared and investigated for their optical and luminescence properties. Judd–Ofelt theory has been used to derive radiative properties for the $^4F_{9/2}$ level of Dy^{3+} ions. The luminescence spectrum of 1.0 mol% Dy_2O_3-doped glass shows intense yellow emission around 572 nm ascribed to $^4F_{9/2} \rightarrow {}^6H_{13/2}$ transition with 78 % branching ratio and emission cross section of the order of 2.48×10^{-21} cm^2. Moreover, the quantum efficiency of the $^4F_{9/2}$ level has been found to be 76 %. The luminescence decay curves for the yellow emission ($^4F_{9/2} \rightarrow {}^6H_{13/2}$) have been measured and analyzed as a function of Dy^{3+} ion concentration. The results revealed that Dy^{3+}-doped phosphate glasses could be useful for yellow laser applications.

1 Introduction

For the past few years, there is rigorous search on trivalent rare-earth (RE^{3+})-doped optical materials for the design and development of lasers, white light phosphors, display devices, etc. [1, 2]. Recently, particular attention has been paid to develop and design yellow laser, which cannot be obtained even with the Ti:Al_2O_3 laser and its second harmonic [3] due to its potential application in a variety of scientific and technological fields. Although laser emission can be obtained by nonlinear processes in blue and yellow regions from the infrared fundamental radiation of solid-state lasers, very few reports are available on direct emission from doped materials, which would simplify such devices. For the first time, Kaminskii et al. [4] demonstrated yellow laser operation in trivalent dysprosium (Dy^{3+})-doped tungstates for $^4F_{9/2} \rightarrow {}^6H_{13/2}$ ($\sim$570 nm) transition, at liquid nitrogen temperature under xenon flash lamp pumping.

Dy^{3+}-doped glasses have been proved to be potential candidates for the development of yellow laser as Dy^{3+} ion exhibits two bands in the blue (470–500 nm) and yellow (570–600 nm) regions, which are due to the $^4F_{9/2} \rightarrow {}^6H_{15/2}$ and $^4F_{9/2} \rightarrow {}^6H_{13/2}$ transitions, respectively. It is well known that $^4F_{9/2} \rightarrow {}^6H_{13/2}$ electric dipole transition is hypersensitive and its intensity strongly depends on the nature of the host, whereas the intensity of $^4F_{9/2} \rightarrow {}^6H_{15/2}$ magnetic dipole transition is less sensitive to the host. Hence, yellow-to-blue (Y/B) intensity ratio could be varied by changing glass composition, Dy_2O_3 concentration, and pump wavelength. Therefore, at a suitable Y/B intensity ratio, Dy^{3+} ions will also generate white light [5]. Further, fluorescence at 1.32 μm originating from the $^4F_{11/2} \rightarrow {}^6H_{9/2}$ transition of the Dy^{3+} ion is used for the fiber amplifiers in the optical transmission system [6]. In addition, the energy levels of Dy^{3+} ion are capable of emitting mid-IR fluorescence at 2.9 and 4.4 μm, which are due to the $^6H_{13/2} \rightarrow {}^6H_{15/2}$ and $^6H_{11/2} \rightarrow {}^6H_{13/2}$ transitions, respectively [6]. However, the choice of appropriate glass matrix with larger concentration of RE^{3+} ions is still a formidable task.

Among different oxide glass hosts such as silicate, borate, and tellurite, phosphate glasses have received a great attention because of their high thermal stability, high transparency, low melting point, high gain density that is due to high solubility for RE^{3+} ions, and low dispersion

K. Linganna · P. Haritha · V. Venkatramu (✉)
Department of Physics, Yogi Vemana University, Kadapa 516 003, India
e-mail: vvramuphd@gmail.com

K. Venkata Krishnaiah · C. K. Jayasankar
Department of Physics, Sri Venkateswara University, Tirupati 517 502, India

[7]. Incorporation of Al_2O_3 into phosphate glass network increases the cross-linking between PO_4 tetrahedral in the glass matrix, which results in moisture free and thermally stable glass with low thermal expansion coefficient that are used for ion-exchange planar waveguide devices. In order to know the local structure, which rules the optical and luminescence properties of RE^{3+} ions in the present glasses, the glasses of similar glass composition doped with Eu^{3+} ions have been prepared for measuring phonon sideband (PSB) spectrum [8] associated with $^7F_0 \rightarrow {}^5D_2$ transition of Eu^{3+} ions. The interest in Eu^{3+} ion as a spectroscopic structural probe is due to its unique electronic structure with non-degenerate ground ($^7F_0$) and first excited ($^5D_0$) state. The PSB spectrum associated with the $^7F_0 \rightarrow {}^5D_2$ transition at around 1,160 cm^{-1} is observed due to symmetric stretching vibrations of the PO_2 groups coupled to the electronic levels of Eu^{3+} ions.

In view of the above importance, it is interesting to study the optical and luminescence properties of Dy^{3+} ions in K–Sr–Al phosphate glasses. The systematic spectroscopic studies that include phonon sideband, absorption, emission, excitation, and decay analysis for the glass samples with different Dy_2O_3 concentrations have been performed. The local structure around RE^{3+} ions has been analyzed by means of the phonon sideband associated with the Eu^{3+}:$^7F_0 \rightarrow {}^5D_2$ transition. The optical and luminescence properties of Dy^{3+} ions in the present glasses have been evaluated, and the experimental results are compared to the theoretical calculations obtained from the Judd–Ofelt (JO) theory [9, 10].

2 Experimental details

The glass compositions in mol%$(59 - x/2)\ P_2O_5 + 17\ K_2O + (15 - x/2)\ SrO + 9\ Al_2O_3 + x\ Dy_2O_3$ (where $x = 0.1$, 0.5, 1.0, 2.0, and 4.0 mol% referred as PKSAD01, PKSAD05, PKSAD10, PKSAD20, and PKSAD40, respectively) have been prepared by conventional melt-quenching technique. Reagent-grade $Al(PO_3)_3$, $Sr(PO_3)_2$, KH_2PO_4, and Dy_2O_3 were taken as starting materials. About 30 g of batch composition was thoroughly crushed in an agate mortar, and this homogeneous mixture was taken in a platinum crucible and melted in an electronic furnace at around 1,100 °C for 1 h 30 min. The melt was then poured into a preheated brass mold and annealed at 450 °C for about 12 h to remove thermal strain and stress. The glass samples were then allowed to cool to room temperature (RT). Similar procedure has been adopted to prepare 1.0 mol% Eu_2O_3-doped glass. The annealed glass samples were polished for optical characterization.

Refractive index measurements were taken using an Abbe refractometer at sodium wavelength (589.3 nm) with 1-bromonaphthalene ($C_{10}H_7Br$) as contact liquid. The density of the glasses was determined by Archimedes' method using distilled water as an immersion liquid. The Raman spectrum is acquired in backscattering configuration under 785 nm laser excitation. Absorption spectrum was recorded using Perkin Elmer Lambda 950 UV–Vis–NIR spectrophotometer with resolution of $\leq$0.05 nm in UV–Vis and $\leq$0.2 nm in NIR regions. Emission, excitation, and lifetime measurements were recorded using Jobin–Yvon Fluorolog-3 spectrofluorometer with resolution of 0.2 nm using xenon arc lamp as an excitation source (450 W). All these measurements were taken at RT.

3 Results and discussion

3.1 Physical properties

Physical parameters such as refractive index, average molecular weight, density, molar volume, concentration, polaron radius, inter-nuclear distance, field strength, dielectric constant, reflection loss, molar refractivity, and electronic polarizability have been determined for PKSAD glasses and are listed in Table 1. As shown in Table 1, it has been found that refractive index and density increase with increase in Dy_2O_3 content as Dy_2O_3 has a high relative molecular mass. The change in molar volume depends on the rates of change in both density and molecular weight. However, the rate of increased molecular weight is greater than the rate of increased density. This would be accompanied by an increase in the molar volume. The molar volume of the glasses increases and then decreases with increase in Dy_2O_3 content. The observed decrease in polaron radius and inter-nuclear distance and increase in field strength with increasing Dy_2O_3 content are due to the increased value of concentration for Dy^{3+} ions. One of the most important properties of materials, which are closely related to their applicability in the field of optics and electronics, is the electronic polarizability. The state of polarizability of the ions can be estimated using Lorentz–Lorenz equation [11]:

$$R_m = \left[\frac{n^2 - 1}{n^2 + 2}\right]\left(\frac{M}{d}\right) = \left[\frac{n^2 - 1}{n^2 + 2}\right]V_m = 4\pi\alpha N/3 \qquad (1)$$

where M is the molecular weight, d is the density, V_m is the molar volume, α is the electronic polarizability, and N is the Avogadro's number. This equation describes the average molar refraction for isotropic substances such as liquids, glasses, and cubic crystals. As shown in Table 1, the values of molar refractivity and electronic polarizability increase with increase in Dy_2O_3 content.

Table 1 Physical properties of Dy^{3+}-doped phosphate glasses

Properties	PKSAD01	PKSAD05	PKSAD10	PKSAD20	PKSAD40
Refractive index (n)	1.510	1.513	1.518	1. 520	1.526
Average molecular weight [M (g mol^{-1})]	125	126	127	129	134
Density [d (g/cc)]	2.69	2.71	2.74	2.80	2.89
Molar volume [V_m (cm^3 mol^{-1})]	46.23	46.33	46.20	46.17	46.15
Concentration [C ($\times 10^{20}$ ions/cc)]	0.03	1.30	2.61	5.22	10.36
Polaron radius [r_p (Å)]	13.60	7.98	6.31	5.02	3.98
Inter-nuclear distance [r_i (Å)]	33.75	19.75	15.65	12.42	9.88
Field strength [F ($\times 10^{15}$ cm^{-2})]	0.02	0.47	0.75	1.20	1.89
Dielectric constant, ε	2.28	2.29	2.30	2.31	2.33
Reflection loss [R (%)]	4.12	4.16	4.23	4.26	4.34
Molar refractivity [R_m (cm^3)]	13.82	13.92	14.00	14.04	14.28
Electronic polarizability [α ($\times 10^{-24}$ cm^3)]	5.49	5.52	5.56	5.57	5.67

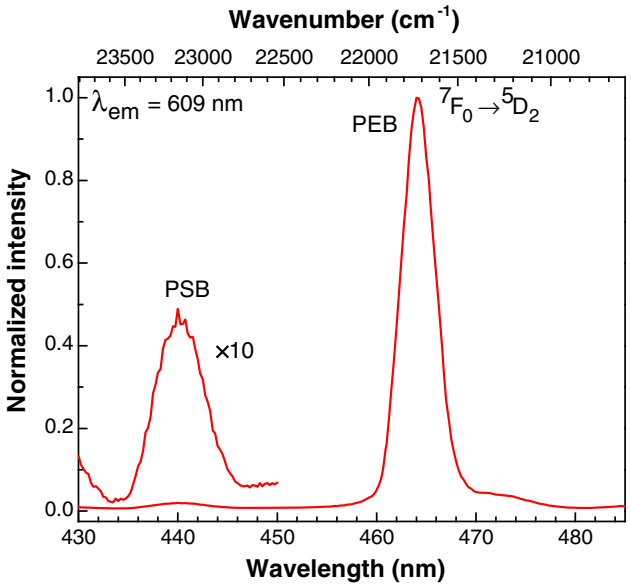

Fig. 1 Excitation spectrum of 1.0 mol% Eu_2O_3-doped PKSAEu glass. The PSB spectrum associated with the PEB is also shown

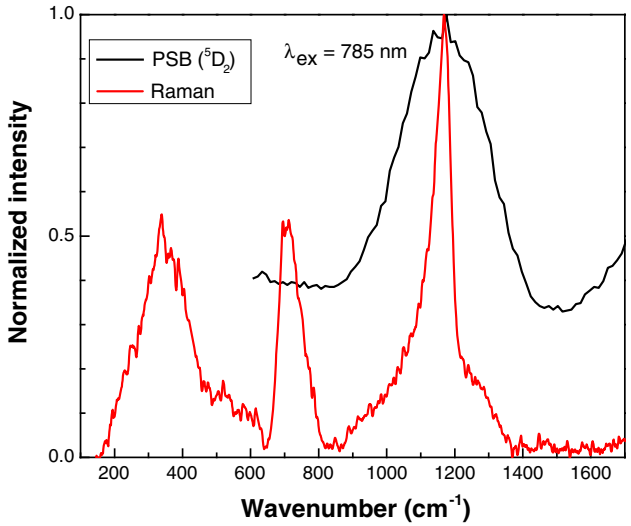

Fig. 2 Comparison of Raman spectrum ($\lambda_{ex} = 785$ nm) of PKSAD10 glass with the PSB spectrum associated with the $^7F_0 \rightarrow {}^5D_2$ PEB of Eu^{3+} in the PKSAEu10 glass. Both are normalized with respect to the maximum peak for comparison

3.2 Phonon sideband spectrum

Figure 1 shows the excitation spectrum of the 1.0 mol% Eu_2O_3-doped phosphate glass of similar base composition (58.5 P_2O_5 + 17 K_2O + 14.5 SrO + 9 Al_2O_3 + 1.0 Eu_2O_3, hereafter referred as PKSAEu10 glass) measured in the range of 430–485 nm by monitoring 609 nm emission that corresponds to $^5D_0 \rightarrow {}^7F_2$ transition. From the excitation spectrum, it is possible to obtain more information about the local structure of Eu^{3+} ions and the nature of their bonds with ligands by analyzing the PSB spectrum, involving simultaneous vibrational and electronic transitions. This excitation spectrum consists of a zero phonon or pure electronic band (PEB), corresponding to $^7F_0 \rightarrow {}^5D_2$ transition; the coupling of the f-electrons with the ligands gives rise to simultaneous transitions between electronic states of the Eu^{3+} ion and vibrational states of the host system and PSB associated with the internal vibrations of the structural groups forming the immediate environment of the Eu^{3+} ions [12]. Taking into account the rather low probability of multiphonon excitation, the difference in energy between the PSB and the PEB corresponds to the energy of the one phonon, associated with the maximum vibrational energy mode coupled to Eu^{3+} ions. The PSB spectrum associated with the $^7F_0 \rightarrow {}^5D_2$ transition (see Fig. 1) consists of an

inhomogeneously broadened, structureless, and intense band at around 1,160 cm^{-1} which is caused by the coupling of symmetric stretching vibrations of the PO_2 groups to the electronic levels of Eu^{3+} ions. Similar PSB spectrum has also been reported in Eu^{3+}-doped metaphosphate [13], fluorometaphosphate [14], and oxyfluoride [15] glasses.

The phonons coupled to Eu^{3+} electronic levels evaluated from PSB spectra are compared with Raman spectrum (see Fig. 2). Raman spectrum that consists of band at around 340 cm^{-1} is assigned to PO_2 and in-chain O–P–O bending and torsional vibrations [16], two bands at around 696 and 1,160 cm^{-1} which are normally observed for metaphosphate glasses [16, 17] and weak band near 1,288 cm^{-1}. The band at around 696 cm^{-1} is assigned to symmetric stretching vibrations of P–O–P linkages [17, 18]. The most intense band near 1,160 cm^{-1} is due to the $(PO_2)_{sym}$ stretching mode of non-bridging terminal oxygens (P=O and $P–O^-$) in Q^2 metaphosphate tetrahedral [19], where the π-bonding is delocalized over the two equivalent P–NBO (P–non-bridging oxygen) bonds, resulting in each having a bond order of ~1.5 [19]. The weak band near 1,288 cm^{-1} is assigned to asymmetric stretching vibrations of PO_2 (terminal P–O bonds) [18, 19].

As shown in Fig. 2, PSB spectrum corresponds well with the Raman spectrum. Comparison between Raman and PSB spectra reveals that intense phonon bands are caused by the symmetric stretching vibrations of PO_2 groups coupled to the Eu^{3+} ions, which are mainly responsible for multiphonon relaxation. The electron–phonon coupling strength (g) is defined as the intensity ratio of the PSB to PEB. For PKSAEu10 glass, the g is 0.031, which is comparable to metaphosphate (0.038) [13] glass but higher than fluorometaphosphate (0.025) [14] glass. It is interesting to note that the oxyfluoride glasses [14, 15] possess lower g value when compared to oxide glasses. The addition of fluoride to the oxide glass leads to ionic bonding due to their incorporation into the immediate environment of the dopant ions. Due to this, oxyfluoride glasses [14, 15] possess lower electron–phonon strength when compared to oxide glasses.

3.3 Judd–Ofelt intensity parameters and radiative properties

The optical absorption spectrum of PKSAD10 glass in the range of 325–2,000 nm is shown in Fig. 3. The spectrum consists of several inhomogeneously broadened transitions from the $^6H_{15/2}$ ground state to the $^6H_{11/2}$, $^6F_{11/2}$, $^6F_{9/2}$, $^6F_{7/2}$, $^6F_{5/2}$, $^6F_{3/2}$, $^4F_{9/2}$, $^4I_{15/2}$, $^4G_{11/2}$, $^4K_{17/2}$, $^4M_{19/2}$, $^4P_{3/2}$, and $^6P_{7/2}$ excited states belonging to the $4f^9$ electronic configuration of Dy^{3+} ion. The measured absorption

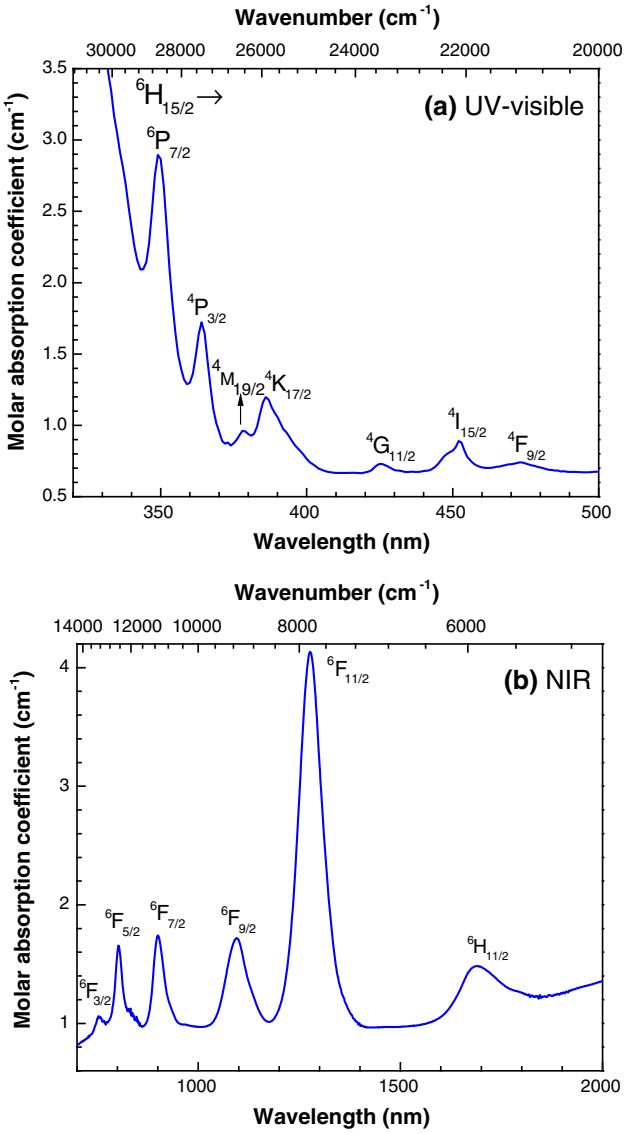

Fig. 3 Absorption spectrum of PKSAD10 glass in **a** UV–visible and **b** NIR regions

spectrum of PKSAD10 glass has been used for the JO analysis. The experimental oscillator strengths (f_{exp}) of various $4f^9$–$4f^9$ transitions of Dy^{3+} ions have been evaluated by integrating each absorption band using the following relation [20]:

$$f_{exp} = 4.318 \times 10^{-9} \int \alpha(\upsilon) d\upsilon \quad (2)$$

where m and e are the mass and charge of an electron, respectively, c is the velocity of light in vacuum, N is the number of Dy^{3+} ions per unit volume, and $\alpha(\upsilon)$ is the molar absorptivity of the corresponding band at an energy υ (in cm^{-1}).

According to the JO theory [9, 10], the calculated oscillator strengths (f_{cal}) of an electric dipole transition $J \rightarrow J'$ is given as follows:

Table 2 Experimental (f_{exp}, $\times 10^{-6}$) and calculated (f_{cal}, $\times 10^{-6}$) oscillator strengths of various transitions of Dy^{3+} ions originating from $^6H_{15/2}$ level in PKSAD10 glass

Transition $^6H_{15/2} \rightarrow$	Wavelength (nm)	PKSAD10	
		f_{exp}	f_{cal}
$^6H_{11/2}$	1,689	1.30	1.47
$^6F_{11/2}$	1,277	8.53	8.51
$^6F_{9/2}$	1,095	2.52	2.57
$^6F_{7/2}$	900	2.08	2.16
$^6F_{5/2}$	802	1.82	1.01
$^6F_{3/2}$	753	0.26	0.19
$^4F_{9/2}$	473	0.19	0.17
$^4I_{15/2}$	452	0.51	0.51
$^4G_{11/2}$	426	0.11	0.08
$^4K_{17/2}$	386	1.66	0.86
$^4M_{19/2}$	378	0.36	0.71
$^4P_{3/2}$	364	1.10	0.32
$^6P_{7/2}$	349	3.19	3.04
Ω_2	10.20×10^{-20} cm^2		
Ω_4	2.14×10^{-20} cm^2		
Ω_6	2.55×10^{-20} cm^2		
$\sigma(N)$[a]	±0.36 (13)		

[a] 'σ' indicates the RMS deviation between experimental and calculated values, and 'N' is the number of levels used in the fit

$$f_{cal} = \frac{8\pi^2 mc\upsilon}{3he^2(2J+1)} \frac{(n^2+2)^2}{9n} \left(e^2 \sum_{\lambda=2,4,6} \Omega_\lambda \left(\psi J || U^\lambda || \psi' J' \right)^2 \right) \quad (3)$$

where $e^2 \sum_{\lambda=2,4,6} \Omega_\lambda (\psi J \| U^\lambda \| \psi' J')^2$ is the line strength of electric dipole transitions, h is the Planck's constant, υ is the wave number of the transition in cm^{-1}, n is the refractive index of the PKSAD10 glass, and J and J' are the total angular momentum for the ground and upper levels, respectively, Ω_λ ($\lambda = 2$, 4, and 6) are the JO parameters that are characteristic of a given RE^{3+} ion, and $\|U^\lambda\|^2$ are the doubly squared reduced matrix elements of the unit tensor operator of the rank $\lambda = 2$, 4, and 6, which are calculated from the intermediate coupling approximation for a transition $\psi J \rightarrow \psi' J'$. The reduced matrix elements, $\|U^\lambda\|^2$ ($\lambda = 2$, 4, and 6), were taken from Ref. [21] since these matrix elements of the unit tensor operator between two energy manifolds in RE^{3+} ion do not vary significantly when it is incorporated in different hosts due to the electrostatic shielding of the *4f* -shell electrons by the closed 5*s*- and 5*p*-shell electrons.

The f_{exp} values evaluated from absorption bands using Eq. (2) are used in Eq. (3). A least square fitting approach was adopted for Eq. (3) to determine Ω_λ ($\lambda = 2$, 4, and 6), which gives the best fit between f_{exp} and f_{cal}. The f_{cal} values are then determined using Ω_λ parameters and Eq. (3). Table 2 presents oscillator strength for observed absorption bands, and it has been found that oscillator strength of electric dipole transition $^6H_{15/2} \rightarrow {}^6F_{11/2}$ is much greater than other transitions, and therefore, the intensity of the corresponding absorption at 1,277 nm is the greatest within the absorption as shown in Fig. 3.

The phenomenological JO intensity parameters ($\times 10^{-20}$ cm^2) for PKSAD10 glass are found to be $\Omega_2 = 10.20$, $\Omega_4 = 2.14$, and $\Omega_6 = 2.55$. The trend of the JO parameters is $\Omega_2 > \Omega_6 > \Omega_4$. Among these JO parameters, Ω_2 is related to the covalency and structural changes in the vicinity of RE^{3+} ion (short-range effect), whereas Ω_4 and Ω_6 are related to the long-range effects and are strongly influenced by the vibrational levels associated with the central RE^{3+} ions bound to the ligand atoms. JO intensity parameters of Dy^{3+} ion and their trend have been compared with reported host matrices [22–30], which are listed in Table 3. It is observed that the present PKSAD10 glass exhibits higher covalency of Dy–O bond and asymmetry around Dy^{3+} ions compared to those of reported Dy^{3+}-doped systems, which include 30 PbO–25 Sb_2O_3–44 B_2O_3–1.0 Dy_2O_3 (PbSBDy10) [22], YAG [23], 92 (Na_2-O + Al_2O_3 + P-$_2O_5$)–7 Al_2O_3–1.0 Dy_2O_3 (NAP) [24], 40 BaO–20 TiO_2–40 SiO_2–1.5 Dy_2O_3 (BTiSDy15) [25], Gd_2SiO_5 [26], 49 B_2O_3 -20 Bi_2O_3–15 Li_2O–10 SrO–5 SrF_2–1.0 Dy_2O_3 (SLBiBDy10) [27], 30 PbO–49 H_3BO_3–10 TiO_2–10 AlF_3–1.0 Dy_2O_3 (L_1BTAFDy) [28], 58.5 P_2O_5–17.0 K_2O–14.5 MgO–9.0 Al_2O_3–1.0 Dy_2O_3 (PKMADy10) [29], and 55.5 P_2O_5–14.0 K_2O–14.5 MgO–9.0 Al_2O_3–6.0 MgF_2–1.0 Dy_2O_3 (PKMFADy10) [29] but lower covalency and higher symmetry compared to 44 P_2O_5–17 K_2O–9 Al_2O_3–23 PbO–6 Na_2O–1.0 Dy_2O_3 (PbPKANDy10) [30] glass. The JO parameters determined from absorption spectrum along with refractive index are used to predict radiative properties such as transition probabilities (A), branching ratios (β_R), and radiative lifetimes (τ_{rad}) of the excited states of Dy^{3+} ions in PKSAD10 glass. These radiative properties predicted by the JO theory are important for the evaluation of the suitability of a material for laser emission. The τ_{rad} for the $^4F_{9/2}$ level of Dy^{3+} ion is found to be 775 μs and is compared to those of reported Dy^{3+}-doped systems (see Table 3). It can be seen that τ_{rad} is comparable to L_1BTAFDy [28] glass but higher than Gd_2SiO_5 [26], SLBiBDy10 [27], and PbPKANDy10 [30] and lower than PbSBDy10 [22], YAG [23], and NAP [24] systems.

The parameter β_R of the luminescence transitions characterizes the lasing power of the transitions. The β_R values for various $^4F_{9/2} \rightarrow {}^6H_J$ (J = 11/2, 13/2, and 15/2) luminescent transitions are predicted to be 8, 75, and 17 %, respectively, for PKSAD10 glass. The experimental branching ratios (β_{exp}) from emission spectrum are determined to be 4, 78, and 18 % for $^4F_{9/2} \rightarrow {}^6H_J$ (J = 11/2,

Table 3 Glass composition, JO intensity parameters ($\times 10^{-20}$ cm^2) and their trend, radiative (τ_{rad}, ms) and experimental (τ_{exp}, ms) lifetime of $^4F_{9/2}$ level, predicted branching ratios (β_R, %), and stimulated emission cross sections ($\sigma(\lambda_p)$, $\times 10^{-21}$ cm^2) of $^4F_{9/2} \rightarrow {}^4I_{13/2}$ transition and Y/B ratios in Dy^{3+}-doped systems

Glass composition	Ω_2	Ω_4	Ω_6	Trend	τ_{rad}	τ_{exp}	β_R	$\sigma(\lambda_p)$	Y/B
PKSAD10 [present work]	10.20	2.14	2.55	$\Omega_2 > \Omega_6 > \Omega_4$	0.78	0.59	75	2.48	3.37
PbSBDy10 [22]	5.81	1.13	2.68	$\Omega_2 > \Omega_6 > \Omega_4$	1.22	0.90	76	–	0.65
Dy:YAG [23]	0.20	1.11	1.46	$\Omega_6 > \Omega_4 > \Omega_2$	2.02	–	51	15.0	–
Dy:NAP [24]	6.68	1.10	1.73	$\Omega_2 > \Omega_6 > \Omega_4$	1.11	1.03	–	3.58	2.90
BTiSDy15 [25]	8.30	1.44	0.99	$\Omega_2 > \Omega_4 > \Omega_6$	–	–	–	–	–
Dy:Gd_2SiO_5 [26]	3.22	2.16	3.76	$\Omega_6 > \Omega_2 > \Omega_4$	0.54	–	54	6.80	–
SLBiBDy10 [27]	4.69	1.46	1.19	$\Omega_2 > \Omega_4 > \Omega_6$	0.14	0.13	–	1.71	0.97
L_1BTAFDy [28]	10.17	4.32	3.27	$\Omega_2 > \Omega_4 > \Omega_6$	0.79	0.20	64	4.35	3.22
PKMADy10 [29]	7.55	2.30	1.70	$\Omega_2 > \Omega_4 > \Omega_6$	–	0.71	59	2.62	1.99
PKMFADy10 [29]	8.40	1.84	1.41	$\Omega_2 > \Omega_4 > \Omega_6$	–	0.79	66	2.49	1.55
PbPKANDy10 [30]	11.74	2.64	2.86	$\Omega_2 > \Omega_6 > \Omega_4$	0.60	0.47	67	5.45	4.50

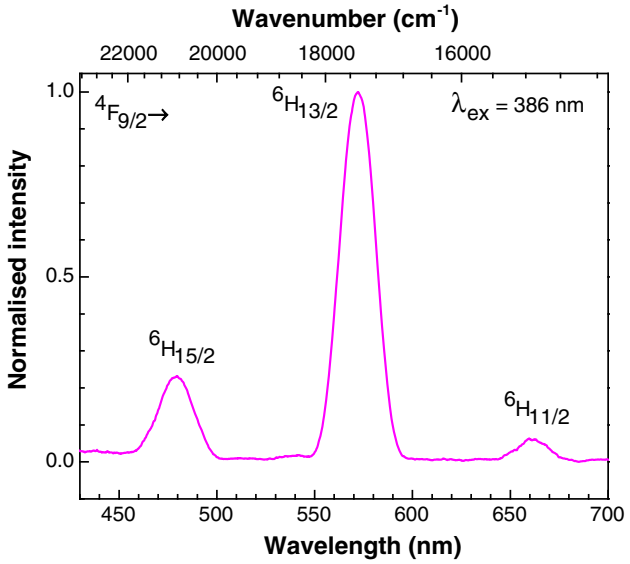

Fig. 4 Luminescence spectrum of PKSAD10 glass obtained under 386 nm excitation

13/2, and 15/2) luminescent transitions, respectively, which are in good agreement with β_R values predicted from the JO theory. It was well established that the transition with β_R value nearly equal to 50 % is a potential laser transition [31]. In the present investigation, $^4F_{9/2} \rightarrow {}^6H_{13/2}$ transition is found to have the highest value of β_R (>75 %) and this transition may therefore be considered as a possible yellow laser transition. Table 3 presents β_R values in different Dy^{3+}-doped host matrices. As shown in Table 3, β_R obtained for present PKSAD10 glass is comparable to PbSBDy10 [22] but higher than YAG [23], Gd_2SiO_5 [26], L_1BTAFDy [28], PKMADy10 [29], PKMFADy10 [29], and PbPKANDy10 [30] systems.

The luminescence spectra were recorded under 386 nm excitation with varying Dy_2O_3 concentration. The spectral shapes and positions are found to be similar for all the measured glasses, and hence, luminescence spectrum for PKSAD10 glass is shown in Fig. 4. From the spectrum, two relatively intense bands at 483 and 572 nm, and a considerable less intense band at 660 nm, have been observed, which are attributed to $^4F_{9/2} \rightarrow {}^6H_{15/2}$, $^4F_{9/2} \rightarrow {}^6H_{13/2}$, and $^4F_{9/2} \rightarrow {}^6H_{11/2}$ transitions, respectively. Owing to small energy gaps between all states lying above 21,000 cm^{-1}, the $^4F_{9/2}$ state is efficiently populated by non-radiative multiphonon relaxation. Then, quite strong yellow and blue luminescence originating from the $^4F_{9/2}$ state is observed. This phenomenon is due to large separation ($\sim$6,000 cm^{-1}) between $^4F_{9/2}$ state and the relatively high phonon cutoff of the host (1,160 cm^{-1}).

One of the most important parameters that characterize the laser performance of a material is stimulated emission cross section [$\sigma(\lambda_p)$], which can be calculated from the luminescence spectrum, and its value signifies the rate of energy extraction from the lasing material. From the measured emission bands, $\sigma(\lambda_p)$ could be estimated by the equation:

$$\sigma(\lambda_p) = \frac{\lambda_p^4}{8\pi c n^2 \Delta\lambda_{eff}} A \quad (4)$$

where c is the velocity of light, n is the refractive index, λ_p is the emission peak wavelength, $\Delta\lambda_{eff}$ is the effective bandwidth obtained by integrating the intensity of the luminescence line shape and dividing it by the intensity at the peak wavelength, and A is the radiative transition probability.

Luminescence properties such as $\Delta\lambda_{eff}$ and $\sigma(\lambda_p)$ for PKSAD10 glass have been evaluated from the luminescence spectrum. The $\Delta\lambda_{eff}$ is obtained to be 19, 21, and 22 nm for

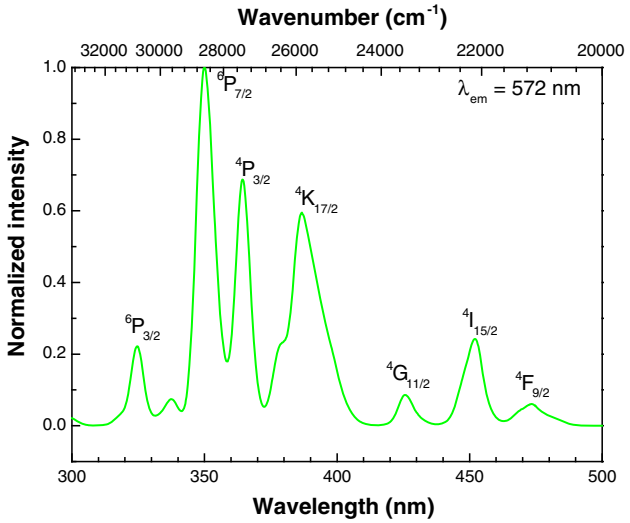

Fig. 5 Excitation spectrum of PKSAD10 glass obtained by monitoring 572 nm emission

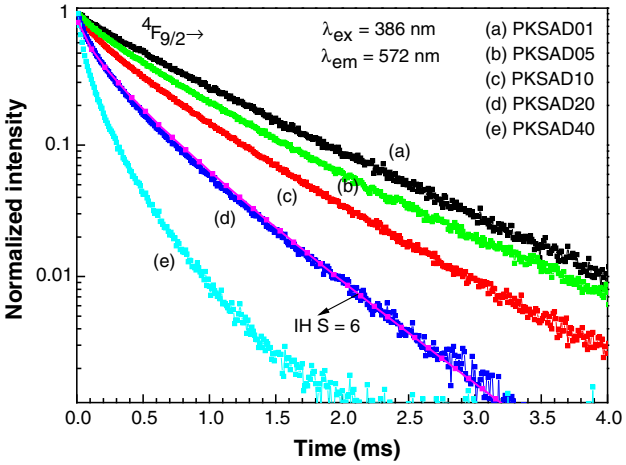

Fig. 6 Decay curves for the $^4F_{9/2}$ level of Dy^{3+} ion for different Dy_2O_3 concentrations in PKSAD glasses. IH fit for $S = 6$ is also shown by *solid lines* for PKSAD glasses

$^4F_{9/2} \rightarrow {}^6H_J$ (J = 11/2, 13/2, and 15/2) transitions, respectively. The $\sigma(\lambda_p)$ ($\times 10^{-21}$ cm^2) for $^4F_{9/2} \rightarrow {}^6H_J$ (J = 11/2, 13/2, and 15/2) transitions has been determined to be 0.32, 2.48, and 0.26, respectively. It has been noticed that $\sigma(\lambda_p)$ is higher for $^4F_{9/2} \rightarrow {}^6H_{13/2}$ transition compared to other transitions. The $\sigma(\lambda_p)$ values of the present study are presented in Table 3 along with reported Dy^{3+}-doped systems. It can be seen that $\sigma(\lambda_p)$ is found to be more or less similar to Dy^{3+}-doped PKMADy10 [29] and PKMFADy10 [29] glasses but lower than YAG [23], NAP [24], Gd_2SiO_5 [26], L_1BTAFDy [28], and PbPKANDy10 [30] and higher than SLBiBDy10 [27] systems.

The Y/B intensity ratio due to $^4F_{9/2} \rightarrow {}^6H_{15/2}$ and $^4F_{9/2} \rightarrow {}^6H_{13/2}$ transitions has been analyzed as a function of Dy_2O_3 content. The $^4F_{9/2} \rightarrow {}^6H_{13/2}$ transition is hypersensitive ($\Delta L = 2$ and $\Delta J = 2$), and its luminescence intensity strongly depends on the host, in comparison with the less sensitive $^4F_{9/2} \rightarrow {}^6H_{15/2}$ transition. The Y/B intensity ratios of all the Dy^{3+}-doped phosphate glasses are in the range of 3.32–3.40 when Dy_2O_3 concentration is increased from 0.1 to 4.0 mol%. It is noticed that Y/B ratio is more or less similar for all the concentrations of Dy^{3+} ions in the present PKSAD glasses, suggesting that the local environment around Dy^{3+} is invariant with varying concentration. Similar results are also observed by Amarnath Reddy et al. [24] in Dy^{3+}-doped NAP glasses. These Y/B ratios are comparable to those obtained for Dy^{3+}-doped L_1BTAFDy10 [28] glass but higher than those obtained for other Dy^{3+}-doped systems which include YAG [23], NAP [24], SLBiBDy10 [27], PKMADy10 [29], and PKMFADy10 [29] and lower than PbPKANDy10 [30]. Comparatively larger Y/B ratios in the present PKSAD glasses suggest the pronounced nature of covalency and asymmetry effects [32]. It is noticed that glasses exhibiting high value of Ω_2 parameter emit relatively high Y/B intensity ratio, which is advantageous for laser operation in the yellow region near 570 nm.

Figure 5 shows the excitation spectrum of the PKSAD10 sample measured by monitoring the emission at 572 nm ($^4F_{9/2} \rightarrow {}^6H_{13/2}$). This spectrum exhibits seven excitation bands in the range from UV (310 nm) to blue (500 nm). The bands in the excitation spectra can be assigned to the transitions from the ground state $^6H_{15/2}$ to higher levels of Dy^{3+}. Among these bands, it is found that the excitation wavelengths of the PKSAD10 glass match well with the emission wavelength of the commercial UV LEDs ($\lambda_{em} = \sim$ 350–410 nm), which could be useful to get Dy^{3+} emissions.

3.4 Decay curve analysis

The decay curves for the $^4F_{9/2}$ level of Dy^{3+} ions in PKSAD glasses have been measured by monitoring 572 nm emission that corresponds to the $^4F_{9/2} \rightarrow {}^6H_{13/2}$ transition and are shown in Fig. 6. As could be observed in the lowest concentration samples ($\leq$0.5 mol%), decay curves is of single exponential nature and become non-exponential with increasing Dy_2O_3 concentration ($\geq$1.0 mol%). The effective lifetime (τ_{eff}) was calculated using the equation:

$$\tau_{eff} = \int \frac{tI(t)dt}{I(t)dt}. \quad (5)$$

The effective lifetime (τ_{eff}) for the $^4F_{9/2}$ level of Dy^{3+} ion in the present PKSAD glasses has been determined to be 746, 729, 590, 443, and 283 μs for 0.1, 0.5, 1.0, 2.0, and 4.0 mol% Dy_2O_3 concentrations, respectively. The τ_{eff}

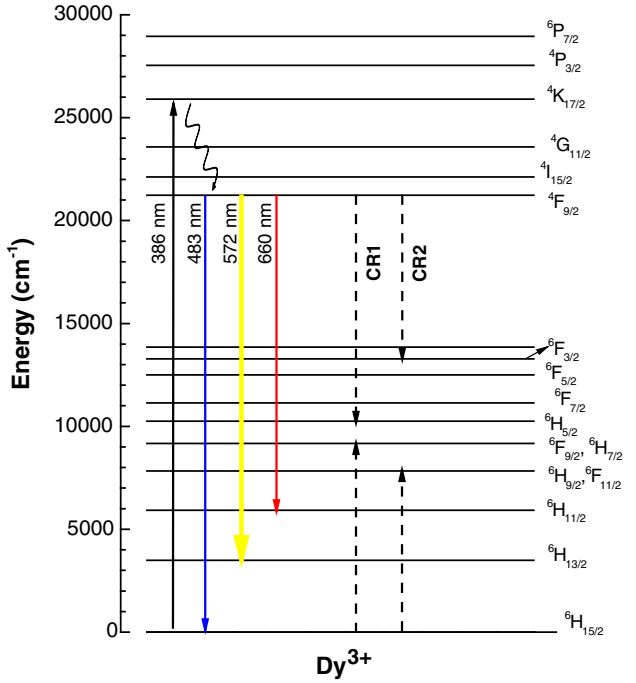

Fig. 7 Partial energy level diagram of Dy^{3+} ions in PKSAD10 glass representing radiative, non-radiative, and possible cross-relaxation channels

value for the PKSAD10 glass is presented in Table 3 along with reported Dy^{3+}-doped systems. It is noticed that τ_{eff} for the present study is more or less similar to PKMADy10 [29], PKMFADy10 [29], and PbPKANDy10 [30] glasses but lower than PbSBDy10 [22] and NAP [24] and higher than SLBiBDy10 [27] and L_1BTAFDy [28] systems. The decrease in lifetime with increase in Dy_2O_3 content is due to non-radiative energy transfer among Dy^{3+} ions through cross-relaxation process [33]. The non-radiative energy transfer probability (W_{NR}) between Dy^{3+} ions can be evaluated using the expression [34]:

$$W_{NR} = \frac{1}{\tau_{eff}} - \frac{1}{\tau_{rad}} \tag{6}$$

The non-radiative relaxation rates of $^4F_{9/2}$ excited are determined to be 50, 80, 400, 970, and 2,240 s^{-1} for 0.1, 0.5, 1.0, 2.0, and 4.0 mol% Dy_2O_3-doped PKSAD glasses, respectively. Notice that W_{NR} increases with increase in Dy_2O_3 concentration. The increase in W_{NR} indicates the presence of non-radiative cross-relaxation channels for $^4F_{9/2}$ level [33] as shown in Fig. 7. A relatively larger phonon cutoff of the PKSAD glass (1,160 cm^{-1}) increases the cross-relaxation processes since energy mismatches can be readily compensated by phonons. The quantum efficiency (η) is defined as the ratio of τ_{exp} and τ_{rad}, which is prerequisite for the laser operation and is given by

$$\eta = \frac{\tau_{exp}}{\tau_{rad}} \tag{7}$$

The η of the $^4F_{9/2}$ level is estimated by assuming similar τ_{rad} for all concentrations of Dy^{3+} ions in the present glasses and are found to be 95, 93, 76, 57, and 36 % for 0.1, 0.5, 1.0, 2.0, and 4.0 mol% Dy_2O_3-doped PKSAD glasses, respectively. It is clearly observed that η is decreasing with increase in Dy^{3+} concentration. Since at low Dy^{3+} concentration, the distance between Dy^{3+} and Dy^{3+} is higher, which leads to low non-radiative energy transfer probability because of low ion–ion interaction, whereas at high Dy^{3+} concentration, the distance between Dy^{3+} and Dy^{3+} becomes lower, which leads more ion–ion interaction consequences higher non-radiative energy transfer probability results low quantum efficiency.

In order to estimate the ion–ion interaction, Inokuti–Hirayama (IH) model [35] has been applied for the luminescence decay curve analysis. The IH model is applicable when the donor–acceptor transfer is faster than migration. The IH model expression is given by

$$I(t) = I_0 \exp\left\{-\left(\frac{t}{\tau_0}\right) - Q\left(\frac{t}{\tau_0}\right)^{3/S}\right\} \tag{8}$$

where $I(t)$ is the luminescence intensity after pulse excitation, τ_0 is the intrinsic lifetime of the donor in the absence of an acceptor, and S can be 6, 8, and 10 for dipole–dipole, dipole–quadrupole, and quadrupole–quadrupole interactions, respectively. The non-exponential decay curves are well fitted to IH model for $S = 6$, which represent the interaction between the donor and the acceptor that is of dipole–dipole type. The similar results have been observed for Dy^{3+}-doped PKMADy [29], PKMFADy [29], and lead bismuthate [36] glasses. The energy transfer parameter (Q) is given as follows:

$$Q = \frac{4\pi}{3}\Gamma\left(1 - \frac{3}{S}\right)N_a R_0^3 \tag{9}$$

where the $\Gamma(x)$ function is equal to 1.77 for dipole–dipole interaction ($S = 6$), 1.43 for dipole–quadrupole interaction ($S = 8$), and 1.3 for quadrupole–quadrupole interaction ($S = 10$). N_a is the concentration of acceptors, which is equal to the concentration of RE^{3+} ions, and R_0 is the critical transfer distance defined as the donor–acceptor separation for which the rate of energy transfer to the acceptors is equal to the rate of intrinsic decay of the donors. The parameter Q is derived in the fitting process, where τ_0 value obtained for 0.1 mol% Dy_2O_3-doped glass was used. The donor–acceptor interaction parameter (C_{DA}) is calculated using the following relation:

$$C_{DA} = \frac{R_0^s}{\tau_0} \tag{10}$$

Results of the fitting for PKSAD glasses using the IH model are given in Table 4 along with reported glasses

Table 4 Dy_2O_3 concentration (C, mol%), energy transfer parameter (Q), critical transfer distance (R_0, Å), and donor–acceptor interaction parameter (C_{DA}, $\times 10^{-41}$ cm^6 s^{-1}) of Dy^{3+} ions in PKSAD glasses

C	PKSAD			PKBAD [37]			PKBFAD [37]			PKBAFD [38]		
	Q	R_0	C_{DA}	Q	R_0	C_{DA}	Q	R_0	C_{DA}	Q	R_0	C_{DA}
1.0	0.20	4.68	1.41	0.55	6.7	1.00	0.61	6.9	1.14	0.40	7.0	13.3
2.0	1.22	6.80	13.25	0.96	6.4	7.30	1.06	6.6	8.60	0.86	7.54	20.7
4.0	2.60	6.97	15.37	–	–	–	–	–	–	–	–	–

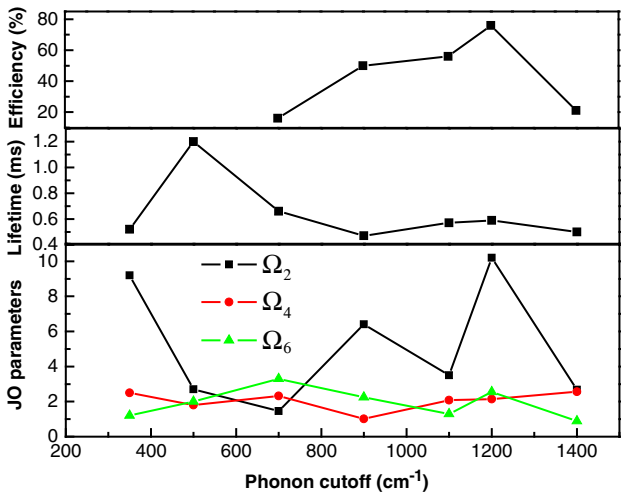

Fig. 8 Variation in JO parameters, lifetime, and quantum efficiency as a function of phonon cutoff in different Dy^{3+}-doped glass hosts

[37, 38]. As shown in Table 4, it is noticed that the parameters Q, R_0, and C_{DA} are changed with Dy_2O_3 concentration, indicating strong dependence on Dy^{3+} ion concentration.

Figure 8 shows the variation in JO parameters, luminescence lifetime, and quantum efficiency with respect to phonon cutoff of various glass compositions, which include chalcogenide [39], fluorozirconate [40], tellurite [41], germanate [42], silicate [43], and borate [44] glasses along with present phosphate glass. As shown in Fig. 8, the higher quantum efficiency has been noticed for the studied phosphate (Sr–K–Al) glass, due to low non-radiative energy transfer probability of phosphate glass (400 s^{-1}) when compared to other reported Dy^{3+}-doped tellurite (1,261 s^{-1}) [41], germanate (1,068 s^{-1}) [42], silicate (771 s^{-1}) [43], and borate (1,565 s^{-1}) [44] glasses. The luminescence lifetime plays a main role to get the higher population at the excited state, which is higher for fluorozirconate glass [40], due to the reduction of OH^- content as well as presence of F^- ions. The studied phosphate glass has moderate lifetime when compared with the other oxide glasses [41–44]. It can be seen that higher value of Ω_2 has been obtained, indicating higher degree of covalency of Dy–O bond and asymmetry around the Dy^{3+} ions in the studied glass composition when compared to other glass systems [39–44].

4 Conclusions

Dy^{3+}-doped K–Sr–Al phosphate glasses have been prepared and characterized through absorption, emission, excitation, and decay curve analysis. The JO parameter Ω_2 is found to be higher, which is an indicative of higher covalency of Dy–O bond and asymmetry around Dy^{3+} ions in the present glasses. Luminescence spectrum of Dy^{3+} ions shows strong band in the yellow region corresponding to $^4F_{9/2} \rightarrow {}^6H_{13/2}$ transition with higher branching ratio of 78 %. The quantum efficiency has been estimated to be 76 % for 1.0 mol% Dy_2O_3-doped phosphate glass, which is higher compared to tellurite (16 %), germanate (50 %), silicate (56 %), and borate (21 %) glasses due to low non-radiative energy transfer probability. The lifetime of $^4F_{9/2}$ level is found to decrease with increasing Dy_2O_3 concentration due to energy transfer between the Dy^{3+} ions, and their interaction is found to be dipole–dipole nature from non-exponential decay curve analysis. The results indicate that Dy^{3+}-doped K–Sr–Al phosphate glasses could be useful for the yellow laser applications.

Acknowledgments Dr. V. Venkatramu is grateful to Council of Scientific and Industrial Research (CSIR), New Delhi, for the sanction of major research project (No. 03(1229)/12/EMR-II, dated 16 April, 2012). This work has also been supported by Mega Project (No. 2009/34/36/BRNS/3174, dated 12 February, 2010) sanctioned to Prof. C.K. Jayasankar through MoU between Sri Venkateswara University, Tirupati, and Bhabha Atomic Research Centre, Mumbai.

References

1. N.S. Singh, R.S. Ningthoujam, M.N. Luwang, S.D. Singh, R.K. Vatsa, Chem. Phys. Lett. **480**, 237 (2009)
2. B. Yan, X. Su, J. Alloys Compd. **431**, 342 (2007)
3. M. Higuchi, R. Sasaki, J. Takahashi, J. Cryst. Growth **311**, 2336 (2009)
4. A. Kaminskii, U. Hömmerich, D. Temple, J.T. Seo, K-i Ueda, S. Bagayev, A. Pavlyulk, Jpn. J. Appl. Phys. **39**, L208 (2000)
5. P. Babu, K.H. Jang, C.S. Rao, L. Shi, C.K. Jayasankar, V. Lavin, H.J. Seo, Opt. Express **19**, 1836 (2011)

6. Y.B. Shin, J. Heo, J. Non-Cryst, Solids **256–257**, 260 (1999)
7. J.H. Campbell, T.I. Suratwala, J. Non-Cryst, Solids **263–264**, 318 (2002)
8. S. Todoroki, K. Hirao, N. Soga, J. Non-Cryst, Solids **143**, 46 (1992)
9. B.R. Judd, Phys. Rev. **127**, 750 (1962)
10. G.S. Ofelt, J. Chem. Phys. **37**, 511 (1962)
11. F. Torres, K. Narita, Y. Benino, T. Fujiwara, T. Komatsu, J. Appl. Phys. **94**, 5265 (2003)
12. V. Venkatramu, D. Navarro-Urrios, P. Babu, C.K. Jayasankar, V. Lavin, J. Non-Cryst, Solids **349**, 105 (2005)
13. P. Babu, H.J. Seo, K.H. Jang, R. Balakrishnaiah, C.K. Jayasankar, A.S. Joshi, J. Phys.: Condens. Matter **17**, 4859 (2005)
14. P. Babu, K.H. Jang, E.S. Kim, R. Vijaya, C.K. Jayasankar, V. Lavin, H.J. Seo, J. Non-Cryst, Solids **357**, 2139 (2011)
15. V. Lavin, P. Babu, C.K. Jayasankar, I.R. Martin, V.D. Rodriguez, J. Chem. Phys. **115**, 10935 (2001)
16. D. llieva, B. Jivov, G. Bogachev, C. Petkov, I. Penkov, Y. Dimitiev, J. Non-Cryst. Solids **283**, 195 (2001)
17. B.N. Nelson, G.J. Exarhos, J. Chem. Phys. **71**, 2739 (1979)
18. G. Poirier, Y. Messaddeq, S.L. Ribeiro, M. Poulain, J. Solid State Chem. **178**, 1533 (2005)
19. J.J. Hudgens, R.K. Brow, D.R. Tallant, S.W. Martin, J. Non-Cryst, Solids **223**, 21 (1998)
20. W.T. Carnall, in: K.A. Gschneidner Jr., L.R. Eyring (Eds.), *Handbook on the Physics and Chemistry of Rare*-Earths (North-Holland Publishing Co., Amsterdam, Vol. **3,** Chapter 24, 1979)
21. C.K. Jayasankar, E. Rukmini, Phys. B **240**, 273 (1997)
22. M.C.S. Reddy, B.A. Rao, M.G. Brik, A.P. Reddy, P.R. Rao, C.K. Jayasankar, N. Veeraiah, Appl. Phys. B **108**, 455 (2012)
23. A. Lupei, V. Lupei, C. Gheorghe, A. Ikesue, M. Enculescu, J. Appl. Phys. **110**, 083120 (2011)
24. A.A. Reddy, M.C. Sekhar, K. Pradeesh, S.S. Babu, G.V. Prakash, J. Mater. Sci. **46**, 2018 (2011)
25. L.L. Martin, P. Haro-González, I.R. Martín, Opt. Mater. **33**, 738 (2011)
26. R. Lisiecki, G. Dominiak-Dzik, P. Solarz, W. Ryba-Romanowski, M. Berkowski, M. Głowacki, Appl. Phys. B **98**, 337 (2010)
27. D. Rajesh, Y.C. Ratnakaram, M. Seshadri, A. Balakrishna, T. Satya krishna, J. Lumin. **132**, 841 (2012)
28. B.C. Jamalaiah, L.R. Moorthy, H.J. Seo, J. Non-Cryst. Solids **358**, 204 (2012)
29. K. Upendra Kumar, C. Srinivasa Rao, C.K. Jayasankar, S. Surendra Babu, J.L. Lucio, H.M.A. Vallejo, M. Alejandrina Martinez Gamez, Phys. Procedia **13**, 70 (2011)
30. K. Linganna, C.S. Srinivasa Rao, C.K. Jayasankar, J. Quant. Spectrosc. Radiat. Transf **118**, 40 (2013)
31. C. Hirayama, F.E. Camp, N.T. Melamid, K.B. Steinbruegge, J. Non-Cryst, Solids **6**, 342 (1971)
32. K. Seneschal, F. Smektala, S. Jiang, T. Luo, B. Bureau, J. Lucas, N. Peyghambarian, J. Non-Cryst, Solids **324**, 179 (2003)
33. M. Klimczak, M. Malinowski, J. Sarnecki, R. Piramidowicz, J. Lumin. **129**, 1869 (2009)
34. R. Reisfeld, E. Greenberg, R. Velapoldi, B. Barnett, J. Chem. Phys. **56**, 1698 (1972)
35. M. Inokuti, F. Hirayama, J. Chem. Phys. **43**, 1978 (1965)
36. W.A. Pisarski, J. Pisarska, R. Lisiecki, G. Dominiak-Dzik, W. Ryba-Romanowski, Chem. Phys. Lett. **531**, 114 (2012)
37. S.S. Babu, P. Babu, C.K. Jayasankar, T. Troster, W. Sievers, G. Wortmann, Opt. Mater. **31**, 624 (2009)
38. R. Praveena, R. Vijaya, C.K. Jayasankar, Spectrochim. Acta A **70**, 577 (2008)
39. G. Tang, Z. Yang, L. Luo, W. Chen, J. Rare Earths **26**, 889 (2008)
40. V.M. Orera, P.J. Alonso, R. Cases, R. Alcala, Phys. Chem. Glasses **29**, 59 (1988)
41. V.K. Rai, S.B. Rai, D.K. Rai, Opt. Commun. **257**, 112 (2006)
42. B. Klimesz, G. Dominiak-Dzik, M. Zelechower, W. Ryba-Romanowski, Opt. Mater. **30**, 1587 (2008)
43. P. Babu, K.H. Jang, E.S. Kim, L. Shi, R. Vijaya, V. Lavín, C.K. Jayasankar, H.J. Seo, J. Non-Cryst, Solids **356**, 236 (2010)
44. K.K. Mahato, A. Rai, S.B. Rai, Spectrochim. Acta A **61**, 431 (2005)